

Geophysical Research Letters®

RESEARCH LETTER

10.1029/2022GL101368

Key Points:

- A transitional stage of the absorption enhancement (E_{abs}) during the evolution of black carbon (BC) was directly observed in the ambient
- By tracking the evolution of fresh BC, the predicted E_{abs} based on the particle-resolved model showed consistent transitional stage
- The secondary inorganic species acted the most critical role in the coating materials to enhance the absorption of BC-containing particles

Supporting Information:

Supporting Information may be found in the online version of this article.

Correspondence to:

X. Yang,
yangx@sustech.edu.cn

Citation:









Zhai, J., Yang, X., Li, L., Ye, X., Chen, J., Fu, T.-M., et al. (2022). Direct observation of the transitional stage of mixing-state-related absorption enhancement for atmospheric black carbon. *Geophysical Research Letters*, 49, e2022GL101368. <https://doi.org/10.1029/2022GL101368>

Received 24 SEP 2022
Accepted 28 NOV 2022

© 2022. The Authors.

This is an open access article under the terms of the [Creative Commons Attribution-NonCommercial-NoDerivs License](https://creativecommons.org/licenses/by-nc-nd/4.0/), which permits use and distribution in any medium, provided the original work is properly cited, the use is non-commercial and no modifications or adaptations are made.

Direct Observation of the Transitional Stage of Mixing-State-Related Absorption Enhancement for Atmospheric Black Carbon

Jinghao Zhai^{1,2} , Xin Yang^{1,2} , Ling Li³ , Xingnan Ye³, Jianmin Chen³ , Tzung-May Fu^{1,2} , Lei Zhu^{1,2} , Huizhong Shen^{1,2} , Jianhuai Ye^{1,2}, Chen Wang^{1,2} , and Shu Tao^{1,2}

¹School of Environmental Science and Engineering, Southern University of Science and Technology, Shenzhen, China, ²Guangdong Provincial Observation and Research Station for Coastal Atmosphere and Climate of the Greater Bay Area, Shenzhen, China, ³Shanghai Key Laboratory of Atmospheric Particle Pollution and Prevention, Department of Environmental Science and Engineering, Fudan University, Shanghai, China

Abstract The addition of coating to the black carbon (BC) enhances its absorption as more light is focused by the coating “lens.” The absorption enhancement factor (E_{abs}) of BC is difficult to quantify due to an inadequate representation of its mixing structure and the interaction with radiation. Here, by tracking the evolution of the fresh BC particles in the ambient, we found a transitional stage of the particle E_{abs} with the non-BC-to-BC mass ratio (R_{BC}) at ~ 2 , below which there were insufficient coating materials to encapsulate the BC core and the absorption enhancement was not significant ($\sim 14\%$). When the $R_{\text{BC}} > \sim 2$, obvious absorption enhancement occurred as the BC cores were fully covered. Secondary inorganic species played the most critical role in the coating materials to enhance the “lensing effect.” We suppose the particle-resolved core-shell Mie model can be applied in the E_{abs} prediction for most cases.

Plain Language Summary Black carbon is the dominant light-absorbing component of atmospheric aerosols, significantly affecting the global climate. In the atmospheric aging process, such as condensation and oxidation, fresh BC is gradually coated. The light absorption of BC is significantly associated with the amount of its coating material since the coating could act as “lens” to refract more light toward the BC core. However, this “lensing effect” for BC particles is poorly quantified, bringing uncertainties when evaluating the aerosol radiative forcing. In this study, we found there was a transitional behavior for the light absorption by BC particles which was related to the particle mixing states. When the non-BC-to-BC mass ratio for particles is larger than 2, the coating materials are insufficient to encapsulate the BC core and cannot act as the coating “lens.” Our study provides a step forward in understanding the global radiation effect of BC.

1. Introduction

Atmospheric BC aerosols, produced through the incomplete combustion of fossil fuel and biomass burning, strongly absorb light across the solar spectrum and exert a positive atmospheric radiative forcing (Ramanathan & Carmichael, 2008). The freshly emitted BC particles with aggregate structures accumulate secondary organic and inorganic coatings during the atmospheric aging processes, affecting their hygroscopicity, atmospheric lifetime, cloud condensation nuclei activity, and potentially their mass absorption cross-section (Knox et al., 2009; Kuwata et al., 2009; Ohata et al., 2016; Yu et al., 2019). With the addition of coating materials to BC, the light absorption of particles can be enhanced through refraction and internal reflections, referred to as the “lensing effect” (Bond et al., 2006; Fuller et al., 1999). Modeling studies based on the core-shell Mie theory, in which assumed spherical BC-containing particles with a core-shell configuration, predicted that the absorption enhancement factor (E_{abs}) caused by the coating “lens” of particles increased with the increasing coating amounts (Bond et al., 2006; Jacobson, 2001). Laboratory studies have observed this lensing-based absorption enhancement of controlled monodisperse BC seeds or sources in the aging condition with either lab-created environments (Cappa et al., 2012; Schnaiter et al., 2005), or ambient air (Peng et al., 2016). However, field observations found both large and minor E_{abs} for BC even though the particle coating amounts were large (Cappa et al., 2019; S. Liu et al., 2015).

During the aging processes, incompletely coated particles could exist and the absorption of BC is constrained by the complex mixing structures of individual particles (Adachi et al., 2010; China et al., 2013). Previous

studies have noticed that the conventional Mie theory calculation that assumes spherical BC-containing particles with a core-shell structure may overestimate the E_{abs} caused by the coating “lens” (D. Liu et al., 2017; Wu et al., 2018). To make more precise predictions of the E_{abs} affected by particle morphology, microscopy techniques that screen the mixing structures of individual BC particles can be used, but have limited quantitative capability and time resolution, and may evaporate semi-volatile materials during the detection (Adachi et al., 2010; China et al., 2013; Turpin et al., 2000). Online techniques and 3D models accounting for the mixing structures of BC were developed to predict the particle E_{abs} (Hu et al., 2021; Wang et al., 2021). Though the adequate representation of the real-world mixing states for particles could increase the accuracy in predicting the absorption by aerosols, the complex mixing structures (attached, embedded, collapsed, etc.) for the incomplete coated particles are difficult to quantify and implement in the global climate and aerosol models. Modeling studies showed that the particle-to-particle heterogeneity in composition had impacts on the population-level E_{abs} (Fierce et al., 2017, 2020; Matsui et al., 2018).

Recently, a particle-resolved method to predict the E_{abs} was developed by considering the distribution of BC coating thickness, which could successfully predict the E_{abs} consistent with the observations (Zhai et al., 2022). In the current study, the same data set was considered and we extended the previous work to a case study that focused on the relationship between particle aging and the E_{abs} . We directly observed a dynamic track of the aging processes for BC particles based on online measurements of absorption enhancement, mixing state, and chemical composition for the ambient particles in Shanghai, China. We demonstrate a transitional stage of the E_{abs} for particles with the non-BC-to-BC mass ratio (R_{BC}) at ~ 2 in the field observation. The absorption enhancement was minor ($\sim 14\%$) when the $R_{\text{BC}} < 2$, as there were insufficient coating materials to encapsulate the BC core. We also consider explicitly the importance of considering mixing state on a per-particle level rather than an ensemble-level perspective. By tracking the evolution of the fresh BC particles, the predicted E_{abs} based on the particle-resolved core-shell Mie theory model showed a consistent transitional stage. The secondary inorganic species played the dominant role in the coating materials to enhance the “lensing effect” of BC-containing particles. Our study directly verified the transitional stage of particle E_{abs} caused by the mixing states in the ambient, which should be considered in predicting the E_{abs} of BC particles.

2. Methods

2.1. Field Measurements

The field observation campaign was performed at Fudan University ($31^{\circ}14'N$, $121^{\circ}29'E$), located in an urban area in Shanghai, China. The sampling time was from 1 January to 19 January 2017. The overview of the field campaign has been introduced elsewhere (Zhai et al., 2022) and the schematic of the experimental setup is provided in the (Figure S1 in Supporting Information S1). The instrumentation system includes the measurements of optical properties, mixing states, and chemical compositions for the ambient particles.

2.1.1. Optical Measurements

Since BC is typically considered refractory, the heating method is therefore used to remove the part of the volatile coating materials and leave behind the non-volatile particle core (Wehner et al., 2002). Evaporation of the non-refractory materials is induced by heating the sampled ambient particles through a thermodenuder (TD). The heating temperature in this work was set at $300^{\circ}C$ to evaporate the volatile coatings of particles. An actuated ball valve was upstream of the TD and switched between the bypass mode and the TD mode on a 10 min cycle. Two sets of TDs were utilized in this work, one was set before the optical detection, and the other was used in the particle sizing system.

A self-built cavity ring-down spectrometer at 532 nm wavelength and an integrating nephelometer (Model 3563, TSI Inc.) were used to detect the extinction coefficient (b_{ext}) and scattering coefficient (b_{scat}) for particles, respectively (Anderson et al., 1996; Anderson & Ogren, 1998; Bond et al., 2009; Li, Chen, et al., 2011). The absorption coefficient (b_{abs}) resulted from deducting the b_{scat} from the corresponding b_{ext} (Onasch et al., 2015). The CRDS-Nephelometer system switched between the bypass unheated and the TD heated particles every 10 min. The absorption enhancement, E_{abs} , was calculated as the ratio between the b_{abs} observed for the ambient particles passing through the bypass line and the b_{abs} observed for particles passing through the TD:

$$E_{\text{abs}} = \frac{(b_{\text{abs, bypass}}(t-1) + b_{\text{abs, bypass}}(t+1))/2}{b_{\text{abs, TD}}(t)} \quad (1)$$

Though thermal desorption has been widely used to separate the coating and core materials of particles, incomplete volatilization of non-BC materials could occur. The effects of residual coatings on the E_{abs} for particles depend on the amounts and optical properties of the residual materials (Cappa et al., 2013; S. Liu et al., 2015). Extremely low volatile species include non-absorbing inorganics (e.g., chlorides and sulfates), and light-absorbing organics (i.e., brown carbon) (Saleh et al., 2014). With the stronger light-absorbing capacity of residual materials, a bigger underestimation could be existed by the observed E_{abs} (S. Liu et al., 2015). However, the light-absorbing organics preferentially absorb at short wavelengths (Andreae & Gelencsér, 2006), and might be insensitive at 532 nm wavelength which we used to detect the absorption coefficient in this study.

2.1.2. Mixing States

A custom-built volatility tandem differential mobility analyzer (V-TDMA) was used to determine the size-resolved aerosol mixing state (Ye et al., 2009). The monodisperse aerosols with mobility diameters of 40, 70, 100, 150, 200, 300, and 350 nm were selected via the upstream differential mobility analyzer (DMA) and were passed to the TD section at 300°C. The residual particles were then sent to the scanning mobility particle sizer (SMPS) system to detect the residual non-volatile particle size distribution. The V-TDMA was operated alternatively between the unheated SMPS mode and the heated DMA-SMPS mode. Non-BC particles that are low-volatile may exist after heating (Cheung et al., 2016). Thus, number fractions of the non-BC-containing particles detected by the single-particle aerosol mass spectrometer (SPAMS) were taken into consideration to reduce the uncertainty brought by the entire evaporation in the heating process (Zhai et al., 2022).

2.1.3. Single-Particle Chemical Compositions

The aerosol chemical compositions were examined by a SPAMS (Hexin Instrument Co., Ltd.). Detailed information about the SPAMS has been reported previously (Li, Huang, et al., 2011; Zhai et al., 2017). Based on the similarities of the mass-to-charge ratio (m/z) and peak intensity, ambient particles were clustered using an adaptive resonance-theory-based neural network (ART-2a) algorithm with a vigilance factor of 0.85, a learning rate of 0.05, and 20 iterations. Elemental carbon ion clusters have been considered important markers for BC-containing particles. According to their mass spectral patterns, the BC-containing particles were furtherly grouped into six particle types (BC-SO₄, BC-NO₃, BC-NH₄, BC-fresh, BC-biomass burning, i.e., BC-BB, BC-OC, BC-oxygenated OC, i.e., BC-OOC). The naming of a particle type is based on some of the dominant chemical species in an attempt to keep the names short. The average mass spectral patterns of each particle type are shown in Figure S2 in Supporting Information S1.

2.2. Model Prediction

2.2.1. Particle-Resolved R_{BC} and E_{abs}

The methodology of the particle-resolved R_{BC} based on the V-TDMA system and the calculation of the particle-resolved E_{abs} has been introduced previously (Zhai et al., 2022). Briefly, assuming that the BC-containing particles exist with a “core-shell” structure, the mass ratio of the volatile coating and non-volatile core of BC-containing particles (R_{BC}) is calculated as:

$$R_{\text{BC}} = \frac{M_{\text{coating}}}{M_{\text{core}}} = \frac{(V_{\text{particle}} - V_{\text{core}}) \rho_{\text{coating}}}{V_{\text{core}} \rho_{\text{core}}} = \frac{(d_{\text{particle}}^3 - d_{\text{core}}^3) \rho_{\text{coating}}}{d_{\text{core}}^3 \rho_{\text{core}}} \quad (2)$$

where M_x , V_x , and ρ_x are the mass, volume, and material density of the coating and core for the BC-containing particles, respectively. The ρ_{coating} is 1.5 g cm⁻³, while the ρ_{core} is 1.8 g cm⁻³ (Cappa et al., 2012). Here, the assumption is based on the core-shell structure of spherical BC-containing particles. Thus, the volume equivalent diameter, which should be put into Equation 2, can be substituted by the particle mobility diameter.

The core-shell Mie theory model is performed to calculate the theoretical E_{abs} for the BC-containing particles. The calculations are adapted from the Fortran code of Bohren and Huffman (1983). Inputs for the model include the refractive indexes of the core and coating materials, the diameters of the overall BC-containing particle and the inner BC core, and the size distribution of the BC-containing particles.

Here, the size of the overall BC particle was the selected diameter by the first DMA in the V-TDMA system, and the size of the inner core was derived either by considering the bulk R_{BC} or by applying the residual particles size

distribution (d_c) from the SMPS system. For the first case, all the BC cores are assumed to be equally coated by the volatile coating materials, and the inner core (d_{core}) is calculated following the equation:

$$d_{\text{core}(1,2)} = \sqrt[3]{\frac{\rho_{\text{coating}}}{(R_{\text{BC}}\rho_{\text{core}} + \rho_{\text{coating}})} d_{\text{particle}}^3} \quad (3)$$

For the second case, the diameter of the BC core was calculated according to the residual particle distribution after heating. By multiplying the d_{particle} by the shrink factor (SF), the resulting $d_{\text{core},2}$, which was also used in the particle-resolved R_{BC} calculation, was applied to the core-shell Mie model. Detailed information about calculation of the particle-resolved R_{BC} and E_{abs} is in Supporting Information S1.

2.2.2. Aggregate Model

The aggregate model used in this work is based on previous studies (Wu et al., 2012, 2018). Briefly, the aging scale of BC aerosol is determined by the mass of BC and non-BC species. The fractal parameters of aggregated BC particles are different in terms of their aging states. The fractal prefactor (k_0) is assumed to be 1.2, and the fractal dimension (D_f) is 1.8, 2.4, and 2.8 for partly coated (including bare), partially encapsulated, and heavily coated states, respectively. The monomer number of the individual BC particles is derived from the BC mass. In the partly coated states, the thickness of the non-BC coating for each monomer can be calculated from the non-BC mass. The superposition T-matrix method, based on the random-orientation cross sections and scattering matrices for particle clusters, was used to calculate the optical properties of particles in the aggregate model (Mackowski & Mishchenko, 2011).

2.3. Other Measurements

The HYSPLIT-4 (Hybrid Single-Particle Lagrangian Integrated Trajectory) model developed by the Air Resources Laboratory of the NOAA (National Oceanic and Atmospheric Administration), USA, was employed to compute hourly resolved 48 hr air mass backward trajectories at 50 m arrival height. The mass concentration of $\text{PM}_{2.5}$ was provided from the Shanghai Pudong Environmental Monitoring Station, which is in the southeast direction and ~ 10 km away from the sampling site.

3. Results

3.1. Dynamic Variation of the E_{abs}

The observed E_{abs} and population-averaged R_{BC} for the total sampling time were reported previously (Zhai et al., 2022). The frequency distribution of the observed E_{abs} is shown in Figure S3 in Supporting Information S1. In this study, a typical case from clean to polluted weather period was selected to study the aging process for the ambient BC-containing particles (1/7–1/8/2017) and a subset of the measured data was re-analyzed and used. The HYSPLIT backward trajectory model was applied (Figure 1a) and showed that the air masses arriving at the sampling site changed suddenly during this sampling case. From 0:00 to 20:00, 1/7/2017, the air masses from the East China Sea were relatively clean (average mass concentration of $\text{PM}_{2.5} \sim 6.9 \mu\text{g m}^{-3}$). Source of the BC-containing particles during this time was dominated by the local emission, which was mainly traffic-related. The air mass trajectories then rapidly changed to the northwest direction at 21:00, 1/7/2017. The changed trajectories were near the ground level (<200 m height) and passed across the intensively industrialized areas in North China Plain, bringing a mass of particles and the mass concentration of $\text{PM}_{2.5}$ increased sharply to $105.0 \mu\text{g m}^{-3}$ at 10:00, 1/8/2017.

Time series was applied to show the time track of the E_{abs} as a function of the population-averaged R_{BC} (Figure 1b). The turning point of the E_{abs} was consistent with the time when the trajectories of air masses changed (1/7/2017 21:00). Before that, the observed E_{abs} of particles dominated by the local emission was 1.14 ± 0.05 and the R_{BC} was 1.23 ± 0.27 on average (Stage 1), which was in accord with the results of fresh traffic emission observed in both laboratory and ambient measurements (D. Liu et al., 2017). As the polluted air mass arrived, a transitional stage was observed during the studied case. The observed R_{BC} sharply increased from ~ 2.53 at 20:00 1/7/2017 to ~ 5.32 at 21:00 1/7/2017. For Stage 2, the observed E_{abs} and R_{BC} of particles increased to 1.91 ± 0.18 and 6.12 ± 1.27 on average, respectively.

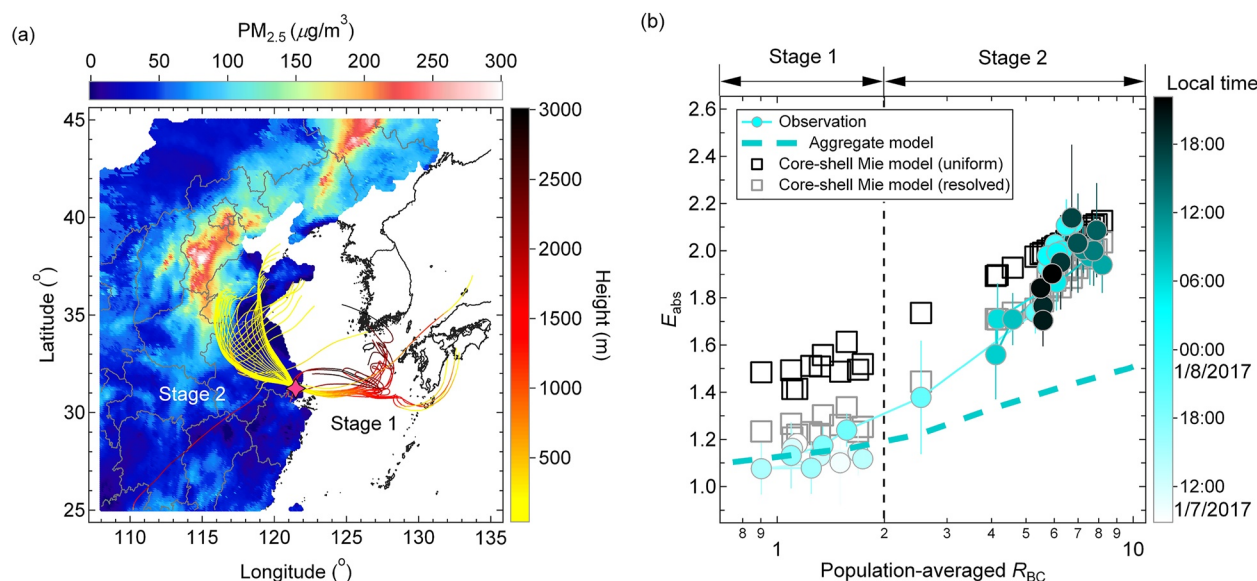


Figure 1. Dynamic aging process of the E_{abs} for BC-containing particles during the studied case. (a) The HYSPLIT 48-hr air mass backward trajectories at 50 m arrival height ending at 07:00 Universal Time Coordinated on 9 January 2017 in Shanghai. Color scales denote the mass concentration of $\text{PM}_{2.5}$ (top) and the height of the trajectories (right) during the case. (b) Time track of the E_{abs} as a function of R_{BC} for the case study. The circles represent the observed results. Core-shell Mie theory model simulations based on the uniform R_{BC} (black squares) and the particle-resolved R_{BC} (gray squares) and the morphology-related aggregate model (blue dash line) are applied. Color scale denotes the time series during the case. Error bars denote a standard deviation.

During Stage 1, the observed E_{abs} of particles increased slightly when the R_{BC} values were small. The assumption of a spherical particle and a core-shell structure may overestimate the E_{abs} of incompletely coated BC in the theoretical calculation from a single-particle level. More realistic mixing structure treatments on the BC-containing particles in the real world may help solve the discrepancy of the E_{abs} . The aggregate model using the superposition T-matrix method was applied to predict the E_{abs} of particles based on their morphological features (Wu et al., 2018). Our direct observation of the E_{abs} in Stage 1 matches with the results from the aggregate model (blue dash line in Figure 1b). As the R_{BC} increased (Stage 2), the predicted E_{abs} for particles by the aggregate model fell behind our observed results. The E_{abs} values using the core-shell Mie theory based on both the classical uniformly distributed coating hypothesis and the particle-resolved coating distribution from our observations were calculated respectively. The scenario of the enhanced absorption by the uniformly distributed coating was modeled based on the bulk R_{BC} to generate the absorption enhancement ($E_{\text{abs, uniform}}$). Under the assumption of equally distributed coating materials across the particle population, the ensemble-average $E_{\text{abs, uniform}}$ values at the R_{BC} below ~ 5 were much higher than our observed results. The SF (detected by the V-TDMA) corrected distribution of particle diameter was put into the core-shell Mie theory to calculate the particle-resolved absorption enhancement ($E_{\text{abs, resolved}}$). Compared to the $E_{\text{abs, uniform}}$, the $E_{\text{abs, resolved}}$ agreed better with the observations. It's also worth noting that, for Stage 1, the results from the aggregate model matched better with the observed values, compared with those from the particle-resolved core-shell Mie model, with Root Mean Square Error (RMSE) of 0.05 for the aggregate model and 0.11 for the particle-resolved core-shell Mie model, respectively. The aggregate model predicts better results when the $R_{\text{BC}} < 2$ as it is based on multiple mixing structures of particles, while the particle-resolved model assumes a single core-shell structure for particles though it has accounted for the particle-to-particle coating distribution. Even so, compared with the conventional core-shell Mie model based on the uniform R_{BC} , we assume the particle-resolved core-shell Mie model is a step forward. The prediction of the $E_{\text{abs, resolved}}$ is still acceptable as the RMSE for the traditional core-shell Mie theory was 0.36 in Stage 1. The dynamic variation of the E_{abs} observed in the field here confirmed that the individual particles changed from incompletely coated (attached, embedded, irregularly coated, etc.) to fully coated structures.

3.2. Evolution of the Fresh BC

The step-up-like E_{abs} with increasing R_{BC} in the rapidly changed weather condition could be a combination of two scenarios. One is the inburst of transported BC particles that were deeply aged with thick coating. The

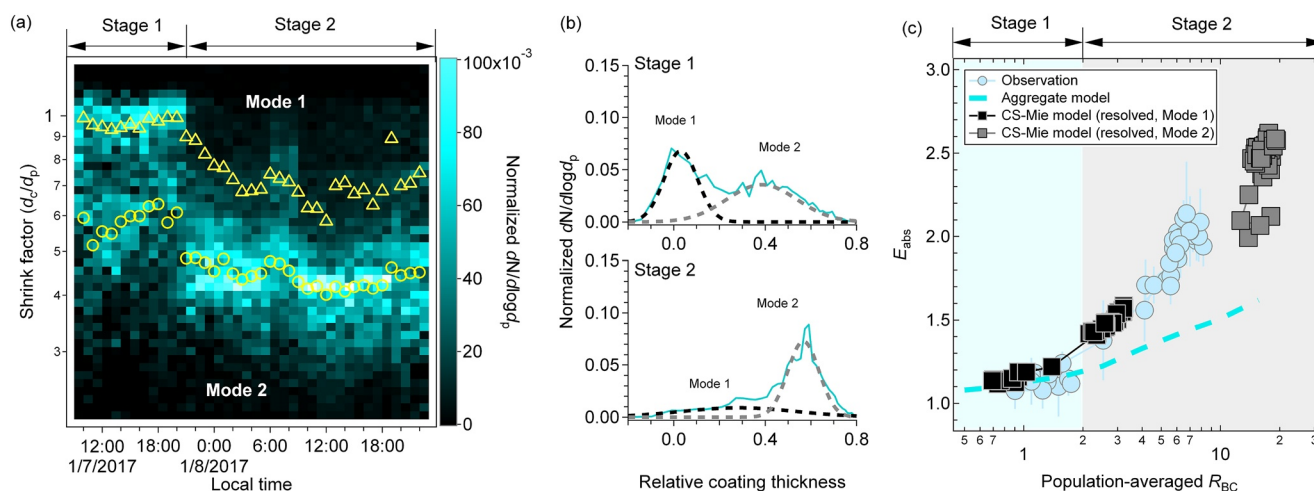


Figure 2. Predicted E_{abs} for different populations of BC-containing particles. (a) The shrink factor (d_c/d_p , $d_p = 150$ nm) distribution during the studied case. Color scale denotes the normalized $dN/d\log d_p$. Bimodal Gaussian fitting is applied to each relative coating thickness (RCT) distribution. Peak values for each mode are marked (yellow triangles for Mode 1 and yellow circles for Mode 2). (b) Average RCT ($1-d_c/d_p$, RCT) distribution for Stage 1 (upper) and Stage 2 (lower) detected by the volatility tandem differential mobility analyzer system during the studied case. Bimodal Gaussian fitting is applied to each RCT distribution. (c) The predicted E_{abs} based on particle-resolved R_{BC} for Mode 1 (black squares) and Mode 2 (gray squares). The circles represent the observed results. The morphology-related aggregate model (blue dashed line) is applied. Error bars denote a standard deviation.

other one is that the local BC particles grew to the magnitude to produce such high E_{abs} with aging. Here, the particle-resolved core-shell Mie model was applied to help distinguish these two scenarios.

During the sampling time, a bimodal distribution of SF , which was defined as the ratio of uncoated particle size (d_c) distribution after heating at 300°C to the selected size (d_p) of unheated particles, was observed (Figures 2a and 2b). The bimodal SF distribution implies heterogeneously distributed coating material across the particle population (Zhai et al., 2022). We attribute the two SF modes to two distinct sources: the local traffic emissions from urban Shanghai, which were dominated by the barely or thinly coated BC particles (i.e., Mode 1), and the long-range transport air masses from northern China that passed across the densely coal-burning and industrial areas, taking along BC-containing particles that are deeply aged with thick coatings (i.e., Mode 2). The distribution of SF can reflect the relative coating thickness (RCT) distribution ($1-d_c/d_p$) reversely. Bimodal Gaussian fitting was applied to each RCT distribution. For Mode 1, the peak value of the RCT distribution increased from 0.04 in Stage 1 to 0.28 in Stage 2 (Figure 2b). The freshly emitted BC particles grew to larger sizes and mixed with the aged BC particles.

To further distinguish and track the aging process of the locally emitted BC particles, we put the SF corrected distribution of particle diameter for the two modes separately into the core-shell Mie theory to calculate the $E_{abs, resolved}$. As the polluted air mass arrived, the $E_{abs, resolved}$ for Mode 1 has the same transitional stage as the observed E_{abs} , that is, at the R_{BC} of ~ 2 (black squares shown in Figure 2c). However, for Mode 2, the $E_{abs, resolved}$ varied in a stable interval (with the averaged value of 2.45 ± 0.15 , gray squares shown in Figure 2c). The E_{abs} and R_{BC} for the aged mode showed little variation with the polluted air mass arriving. We suppose the time track of the fresh mode (Mode 1) is direct proof of the local BC particles aging from the incomplete coating to the fully coated morphology observed in the field measurements.

3.3. Chemical Compositions of Individual BC-Containing Particles

Single-particle chemical compositions for the BC-containing particles also showed a step-up-like behavior during the studied case (1/7–1/8/2017). The fresh BC particles (BC-fresh type) classified from the single-particle mass spectrometry are characterized by the carbon clusters ($C_n^{+/-}$, usually $n > 6$), which is a typical mass pattern from the fresh BC emission (Zhai et al., 2015). Time series of the chemical compositions for particles verified that BC-fresh accounted for $\sim 35\%$ in proportion in the beginning stage of clean weather (Figure 3a). With the air mass trajectory changing, the fraction of BC-fresh decreased to $\sim 10\%$, while the BC-OOC fraction increased by $\sim 100\%$. For the inorganic groups, the BC- SO_4 type presented a significant increase from $\sim 10\%$ (Stage 1) to

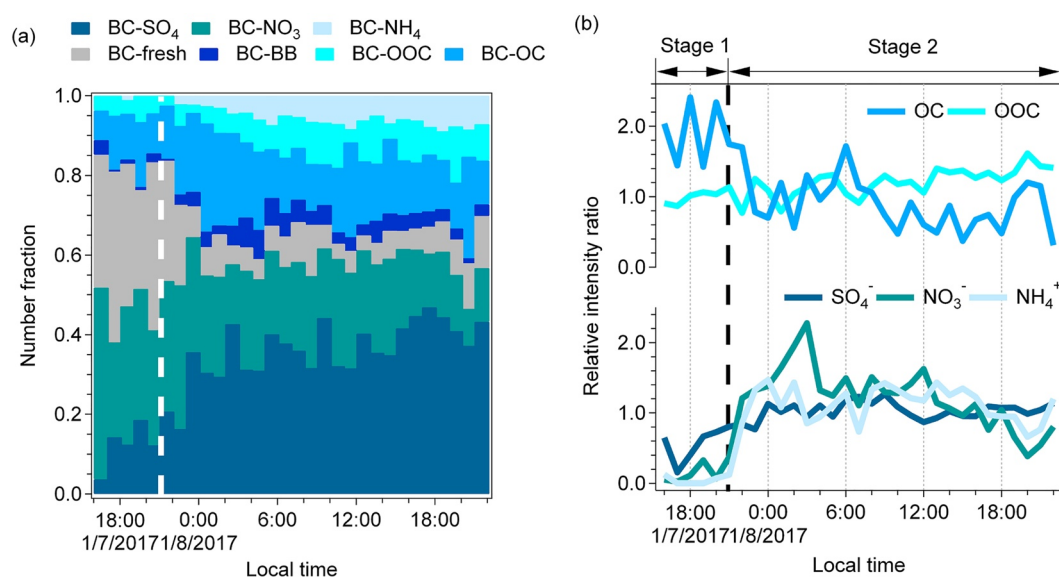


Figure 3. Chemical analysis of the BC-containing particles detected by the single-particle aerosol mass spectrometer (SPAMS). (a) Number fractions of different BC-containing types of particles during the case. (b) Time series of the relative intensity ratio for the specific components in BC-fresh particles. The relative intensity ratio refers to the ratio of relative intensity during the case to the average relative intensity during the whole sampling period. Here, OC is the sum of the representative organic species (m/z 29 [$C_2H_3^+$], 29 [$C_2H_5^+$], 51 [$C_4H_3^+$], 77 [$C_6H_5^+$], -26 [CN^-]), OOC represents the sum of the oxygenated organic species (m/z 43 [CH_3CO^+], -57 [$C_2HO_2^-$], -89 [$C_2O_4H^-$]), SO_4^- represents m/z -97 [SO_4^-], NO_3^- represents m/z -62 [NO_3^-], and NH_4^+ represents m/z 18 [NH_4^+].

~50% (Stage 2). In comparison, the fraction of BC- NO_3 decreased by ~30%. Guo et al. (2014) reported that in urban areas, sulfate forms primarily through the atmospheric oxidation of SO_2 which was emitted mainly from coal-burning and industrial sources, while nitrate derives from NO_x which was emitted mainly from the local vehicles and power plants. We attribute the increased fraction of BC- SO_4 to the regional transport of the aged particles.

We further analyzed the relative signal intensity of specific components in terms of BC-fresh. The relative intensity ratio (relative intensity during the case/average relative intensity for the whole sampling period) was used to uniform the intensity range for different species. The sum of relative signal intensity for typical species (at specific m/z) was used to represent OC (m/z 29 [$C_2H_3^+$], 29 [$C_2H_5^+$], 51 [$C_4H_3^+$], 77 [$C_6H_5^+$], -26 [CN^-]) and OOC (m/z 43 [CH_3CO^+], -57 [$C_2HO_2^-$], -89 [$C_2O_4H^-$]) in fresh BC particles, while that of m/z -97 [SO_4^-], -62 [NO_3^-], and 18 [NH_4^+] were selected to represent the sulfate, nitrate, and ammonium, respectively (Figure 3b). The inorganic species increased markedly with the air mass trajectory changing, indicating that the secondary inorganic species could be the key factor in the rapid increase of the E_{abs} for BC particles in their aging evolution. Compared to the markable increment of the inorganic species, the relative intensity ratio of OOC steadily went up during the BC evolution (~30% increment), which was independent of the different air masses. The signal intensity of OC decreased by ~50% as the air mass changed. These less oxygenated OC species could be the primarily co-emitted components with fresh BC particles (Zhai et al., 2017).

Chemical compositions of coatings can affect BC's morphology and mixing state. It has been reported that the intermediate-volatility chemicals produce concave junctions in between monomers, resulting in prompt restructuring of BC over the uniform coatings on the aggregates produced by the low-volatility materials (Chen et al., 2018). In this study, the secondary sulfate was dominated in the coating materials, and the reconstruction of the aggregates was slow. In this way, the transitional stage of BC might be earlier if the coating materials were dominated by organic species.

4. Conclusions and Discussions

From a case study of the field measurements in which BC particles showed dramatic variation in mixing states, we found a transitional stage at $R_{BC} \sim 2$ to constrain the mixing structures of BC particles, which should be considered in predicting the BC absorption enhancement factor. When the $R_{BC} < \sim 2$, the coating materials for particles were insufficient to encapsulate the BC core and the E_{abs} were small. When the $R_{BC} > \sim 2$, the E_{abs} increased with increasing R_{BC} as BC cores were mostly fully covered by coating materials at this stage. The direct observations and improved optical model simulations presented in this work highlight the importance of particle-resolved mixing state on the E_{abs} of BC particles as well as the global radiative forcing assessment of BC aerosols.

Multiple studies sampled both in the field and laboratory have verified the incompletely coated structures (attached, embedded, collapsed, etc.) of BC-containing particles. Models based on such morphological features predict consistent results with the observed values. Though the adequate representation of the real-world complexity of the aerosol mixing state could increase the accuracy in predicting the aerosols, the complex mixing structures for the incomplete coated particles are difficult to quantify and implement in the large-scale climate and aerosol models in terms of the radiative absorption of aerosols. Here, we assume that the applicable range of this aggregate model in predicting the absorption enhancement should be $R_{BC} < \sim 2$ (before the transitional stage), above which particles age to a fully coated structure and the core-shell Mie theory could be satisfied to predict the E_{abs} of particles. It's worth noting that, it has been found the heterogeneity of R_{BC} within a particle population could lead to the discrepancy between the observed and predicted E_{abs} . Here, we suppose the single mechanism of the particle-resolved mixing state could help solve most cases in the absorption enhancement prediction. Thus, both the morphology-related E_{abs} and the coating heterogeneity influenced E_{abs} have indicated that the mixing state of particles should be better resolved in the large-scale models to add confidence when evaluating the aerosol radiation effect.

Data Availability Statement

The original code used for the Mie theory calculation is in Bohren and Huffman (1983). The method and code of the aggregate model are adapted from Wu et al., 2018. The ART-2a code used for the single-particle mass spectra clustering is available at <https://doi.org/10.5281/zenodo.7092324>.

References

- Adachi, K., Chung, S. H., & Buseck, P. R. (2010). Shapes of soot aerosol particles and implications for their effects on climate. *Journal of Geophysical Research*, 115(D15), D15206. <https://doi.org/10.1029/2009JD012868>
- Anderson, T. L., Covert, D. S., Marshall, S. F., Laucks, M. L., Charlson, R. J., Waggoner, A., et al. (1996). Performance characteristics of a high-sensitivity, three-wavelength, total scatter/backscatter Nephelometer. *Journal of Atmospheric and Oceanic Technology*, 13(5), 967–986. <https://doi.org/10.1175/1520-0426>
- Anderson, T. L., & Ogren, J. A. (1998). Determining aerosol radiative properties using the TSI 3563 integrating Nephelometer. *Aerosol Science and Technology*, 29(1), 57–69. <https://doi.org/10.1080/02786829808965551>
- Andreae, M. O., & Gelencsér, A. (2006). Black carbon or Brown carbon? The nature of light-absorbing carbonaceous aerosols. *Atmospheric Chemistry and Physics*, 6(10), 3131–3148. <https://doi.org/10.5194/acp-6-3131-2006>
- Bohren, C. F., & Huffman, D. R. (1983). Absorption and scattering of light by small particles. <https://doi.org/10.1002/9783527618156>
- Bond, T. C., Covert, D. S., & Müller, T. (2009). Truncation and angular-scattering corrections for absorbing aerosol in the TSI 3563 Nephelometer. *Aerosol Science and Technology*, 43(9), 866–871. <https://doi.org/10.1080/02786820902998373>
- Bond, T. C., Habib, G., & Bergstrom, R. W. (2006). Limitations in the enhancement of visible light absorption due to mixing state. *Journal of Geophysical Research*, 111(D20), D20211. <https://doi.org/10.1029/2006jd007315>
- Cappa, C. D., Onasch, T. B., Massoli, P., Worsnop, D. R., Bates, T. S., Cross, E. S., et al. (2012). Radiative absorption enhancements due to the mixing state of atmospheric black carbon. *Science*, 337(6098), 1078–1081. <https://doi.org/10.1126/science.1223447>
- Cappa, C. D., Onasch, T. B., Massoli, P., Worsnop, D. R., Bates, T. S., Cross, E. S., et al. (2013). Response to Comment on “Radiative absorption enhancements due to the mixing state of atmospheric black carbon”. *Science*, 339(6118), 2. <https://doi.org/10.1126/science.1230260>
- Cappa, C. D., Zhang, X. L., Russell, L. M., Collier, S., Lee, A. K. Y., Chen, C. L., et al. (2019). Light absorption by ambient black and Brown carbon and its dependence on black carbon coating state for two California, USA, cities in winter and summer. *Journal of Geophysical Research*, 124(3), 1550–1577. <https://doi.org/10.1029/2018jd029501>
- Chen, C., Enekwizu, O. Y., Fan, X. L., Dobrzanski, C. D., Ivanova, E. V., Ma, Y., et al. (2018). Single parameter for predicting the morphology of atmospheric black carbon. *Environmental Science & Technology*, 52(24), 14169–14179. <https://doi.org/10.1021/acs.est.8b04201>
- Cheung, H. H. Y., Tan, H., Xu, H., Li, F., Wu, C., Yu, J. Z., & Chan, C. K. (2016). Measurements of non-volatile aerosols with a VTDMA and their correlations with carbonaceous aerosols in Guangzhou, China. *Atmospheric Chemistry and Physics*, 16(13), 8431–8446. <https://doi.org/10.5194/acp-16-8431-2016>
- China, S., Mazzoleni, C., Gorkowski, K., Aiken, A. C., & Dubey, M. K. (2013). Morphology and mixing state of individual freshly emitted wildfire carbonaceous particles. *Nature Communications*, 4(1), 2122. <https://doi.org/10.1038/ncomms3122>

Acknowledgments

This work was supported by the Department of Science and Technology of Guangdong Province (2020B1111360001, 2021B1212050024, 2020B1515130003), the National Natural Science Foundation of China (41827804), and the Department of Education of Guangdong Province (2021KCXTD004).

- Fierce, L., Onasch, T. B., Cappa, C. D., Mazzoleni, C., China, S., Bhandari, J., et al. (2020). Radiative absorption enhancements by black carbon controlled by particle-to-particle heterogeneity in composition. *Proceedings of the National Academy of Sciences of the United States of America*, *117*(10), 5196–5203. <https://doi.org/10.1073/pnas.1919723117>
- Fierce, L., Riemer, N., & Bond, T. C. (2017). Toward reduced representation of mixing state for simulating aerosol effects on climate. *Bulletin of the American Meteorological Society*, *98*(5), 971–980. <https://doi.org/10.1175/bams-d-16-0028.1>
- Fuller, K. A., Malm, W. C., & Kreidenweis, S. M. (1999). Effects of mixing on extinction by carbonaceous particles. *Journal of Geophysical Research*, *104*(D13), 15941–15954. <https://doi.org/10.1029/1998jd100069>
- Guo, S., Hu, M., Zamora, M. L., Peng, J., Shang, D., Zheng, J., et al. (2014). Elucidating severe urban haze formation in China. *Proceedings of the National Academy of Sciences of the United States of America*, *111*(49), 17373–17378. <https://doi.org/10.1073/pnas.1419604111>
- Hu, K., Liu, D., Tian, P., Wu, Y., Deng, Z., Wu, Y., et al. (2021). Measurements of the diversity of shape and mixing state for ambient black carbon particles. *Geophysical Research Letters*, *48*(17). <https://doi.org/10.1029/2021gl094522>
- Jacobson, M. Z. (2001). Strong radiative heating due to the mixing state of black carbon in atmospheric aerosols. *Nature*, *409*(6821), 695–697. <https://doi.org/10.1038/35055518>
- Knox, A., Evans, G. J., Brook, J. R., Yao, X., Jeong, C. H., Godri, K. J., et al. (2009). Mass absorption cross-section of ambient black carbon aerosol in relation to chemical age. *Aerosol Science and Technology*, *43*(6), 522–532. <https://doi.org/10.1080/02786820902777207>
- Kuwata, M., Kondo, Y., & Takegawa, N. (2009). Critical condensed mass for activation of black carbon as cloud condensation nuclei in Tokyo. *Journal of Geophysical Research*, *114*(D20), D20202. <https://doi.org/10.1029/2009jd012086>
- Li, L., Chen, J., Chen, H., Yang, X., Tang, Y., & Zhang, R. (2011). Monitoring optical properties of aerosols with cavity ring-down spectroscopy. *Journal of Aerosol Science*, *42*(4), 277–284. <https://doi.org/10.1016/j.jaerosci.2011.02.001>
- Li, L., Huang, Z., Dong, J., Li, M., Gao, W., Nian, H., et al. (2011). Real time bipolar time-of-flight mass spectrometer for analyzing single aerosol particles. *International Journal of Mass Spectrometry*, *303*(2–3), 118–124. <https://doi.org/10.1016/j.ijms.2011.01.017>
- Liu, D., Whitehead, J., Alfarra, M. R., Reyes-Villegas, E., Spracklen, D. V., Reddington, C. L., et al. (2017). Black-carbon absorption enhancement in the atmosphere determined by particle mixing state. *Nature Geoscience*, *10*(3), 184–188. <https://doi.org/10.1038/ngeo2901>
- Liu, S., Aiken, A. C., Gorkowski, K., Dubey, M. K., Cappa, C. D., Williams, L. R., et al. (2015). Enhanced light absorption by mixed source black and brown carbon particles in UK winter. *Nature Communications*, *6*(1), 8435. <https://doi.org/10.1038/ncomms9435>
- Mackowski, D. W., & Mishchenko, M. I. (2011). A multiple sphere T-matrix Fortran code for use on parallel computer clusters. *Journal of Quantitative Spectroscopy & Radiative Transfer*, *112*(13), 2182–2192. <https://doi.org/10.1016/j.jqsrt.2011.02.019>
- Matsui, H., Hamilton, D. S., & Mahowald, N. M. (2018). Black carbon radiative effects highly sensitive to emitted particle size when resolving mixing-state diversity. *Nature Communications*, *9*(1), 3446. <https://doi.org/10.1038/s41467-018-05635-1>
- Ohata, S., Schwarz, J. P., Moteki, N., Koike, M., Takami, A., & Kondo, Y. (2016). Hygroscopicity of materials internally mixed with black carbon measured in Tokyo. *Journal of Geophysical Research*, *121*(1), 362–381. <https://doi.org/10.1002/2015jd024153>
- Onasch, T. B., Massoli, P., Kebedian, P. L., Hills, F. B., Bacon, F. W., & Freedman, A. (2015). Single scattering albedo monitor for airborne particulates. *Aerosol Science and Technology*, *49*(4), 267–279. <https://doi.org/10.1080/02786826.2015.1022248>
- Peng, J., Hu, M., Guo, S., Du, Z., Zheng, J., Shang, D., et al. (2016). Markedly enhanced absorption and direct radiative forcing of black carbon under polluted urban environments. *Proceedings of the National Academy of Sciences of the United States of America*, *113*(16), 4266–4271. <https://doi.org/10.1073/pnas.1602310113>
- Ramanathan, V., & Carmichael, G. (2008). Global and regional climate changes due to black carbon. *Nature Geoscience*, *1*(4), 221–227. <https://doi.org/10.1038/ngeo156>
- Saleh, R., Robinson, E. S., Tkacik, D. S., Ahern, A. T., Liu, S., Aiken, A. C., et al. (2014). Brownness of organics in aerosols from biomass burning linked to their black carbon content. *Nature Geoscience*, *7*(9), 647–650. <https://doi.org/10.1038/ngeo2220>
- Schnaier, M., Linke, C., Mohler, O., Naumann, K. H., Saathoff, H., Wagner, R., et al. (2005). Absorption amplification of black carbon internally mixed with secondary organic aerosol. *Journal of Geophysical Research*, *110*(D19), D19204. <https://doi.org/10.1029/2005jd006046>
- Turpin, B. J., Saxena, P., & Andrews, E. (2000). Measuring and simulating particulate organics in the atmosphere: Problems and prospects. *Atmospheric Environment*, *34*(18), 2983–3013. [https://doi.org/10.1016/s1352-2310\(99\)00501-4](https://doi.org/10.1016/s1352-2310(99)00501-4)
- Wang, Y., Li, W., Huang, J., Liu, L., Pang, Y., He, C., et al. (2021). Nonlinear enhancement of radiative absorption by black carbon in response to particle mixing structure. *Geophysical Research Letters*, *48*(24), e2021GL096437. <https://doi.org/10.1029/2021gl096437>
- Wehner, B., Philippin, S., & Wiedensohler, A. (2002). Design and calibration of a thermodenuder with an improved heating unit to measure the size-dependent volatile fraction of aerosol particles. *Journal of Aerosol Science*, *33*(7), 1087–1093. [https://doi.org/10.1016/s0021-8502\(02\)00056-3](https://doi.org/10.1016/s0021-8502(02)00056-3)
- Wu, Y., Cheng, T., Liu, D., Allan, J. D., Zheng, L., & Chen, H. (2018). Light absorption enhancement of black carbon aerosol constrained by particle morphology. *Environmental Science & Technology*, *52*(12), 6912–6919. <https://doi.org/10.1021/acs.est.8b00636>
- Wu, Y., Gu, X., Cheng, T., Xie, D., Yu, T., Chen, H., & Guo, J. (2012). The single scattering properties of the aerosol particles as aggregated spheres. *Journal of Quantitative Spectroscopy & Radiative Transfer*, *113*(12), 1454–1466. <https://doi.org/10.1016/j.jqsrt.2012.03.015>
- Ye, X., Chen, T., Hu, D., Yang, X., Chen, J., Zhang, R., et al. (2009). A multifunctional HTDMA system with a robust temperature control. *Advances in Atmospheric Sciences*, *26*(6), 1235–1240. <https://doi.org/10.1007/s00376-009-8134-3>
- Yu, P., Toon, O. B., Bardeen, C. G., Zhu, Y., Rosenlof, K. H., Portmann, R. W., et al. (2019). Black carbon lofts wildfire smoke high into the stratosphere to form a persistent plume. *Science*, *365*(6453), 587–590. <https://doi.org/10.1126/science.aax1748>
- Zhai, J., Lu, X., Li, L., Zhang, Q., Zhang, C., Chen, H., et al. (2017). Size-resolved chemical composition, effective density, and optical properties of biomass burning particles. *Atmospheric Chemistry and Physics*, *17*(12), 7481–7493. <https://doi.org/10.5194/acp-17-7481-2017>
- Zhai, J., Wang, X., Li, J., Xu, T., Chen, H., Yang, X., & Chen, J. (2015). Thermal desorption single particle mass spectrometry of ambient aerosol in Shanghai. *Atmospheric Environment*, *123*, 407–414. <https://doi.org/10.1016/j.atmosenv.2015.09.001>
- Zhai, J., Yang, X., Li, L., Bai, B., Liu, P., Huang, Y., et al. (2022). Absorption enhancement of black carbon aerosols constrained by mixing-state heterogeneity. *Environmental Science & Technology*, *56*(3), 1586–1593. <https://doi.org/10.1021/acs.est.1c06180>